ACS APPLIED MATERIALS & INTERFACES

Research Article

www.acsami.org

Transparent Conductive Oxide-Free Perovskite Solar Cells with PEDOT:PSS as Transparent Electrode

Kuan Sun,[†,‡] Pengcheng Li,[†] Yijie Xia,[†] Jingjing Chang,[†] and Jianyong Ouyang*[,†]

[†]Department of Materials Science & Engineering, National University of Singapore, 7 Engineering Drive 1, Singapore 117574

[‡]School of Power Engineering, Chongqing University, 174 Shazhengjie, Shapingba, Chongqing 400044, China

Supporting Information

ABSTRACT: Perovskite solar cells (PSCs) have been attracting considerable attention because of their low fabrication cost and impressive energy conversion efficiency. Most PSCs are built on transparent conductive oxides (TCOs) such as fluorine-doped tin oxide (FTO) or indium tin oxide (ITO), which are costly and rigid. Therefore, it is significant to explore alternative materials as the transparent electrode of PSCs. In this study, highly conductive and highly transparent poly(3,4-ethylenedioxythiophene):polystyrenesulfonate (PEDOT:PSS) films were investigated as the transparent electrode of both rigid and flexible PSCs. The conductivity of PEDOT:PSS films on rigid glass or flexible poly(ethylene terephthalate) (PET) substrate is significantly enhanced through a treatment with methanesulfonic acid (MSA). The optimal power conversion efficiency (PCE) is close to 11% for the rigid PSCs with an MSA-treated PEDOT:PSS film as the transparent electrode on glass, and it is more than 8% for the flexible PSCs with a MSA-treated PEDOT:PSS film as the transparent electrode on PET. The flexible PSCs exhibit excellent mechanical flexibility in the bending test.

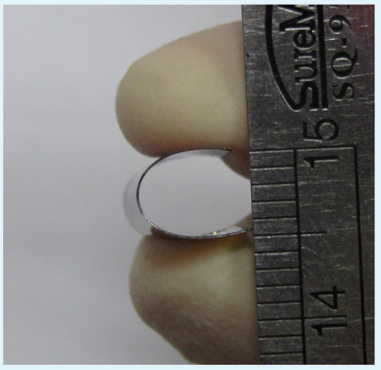

KEYWORDS: *perovskite solar cell, PEDOT:PSS, transparent electrode, flexible solar cell, interface engineering*

1. INTRODUCTION

Perovskite solar cells have been attracting considerable attention because of their low fabrication cost and impressive energy conversion efficiency. They can be fabricated by solution processing.[1] The planar perovskite solar cells do not have a scaffold oxide layer. They could thus be manufactured by a roll-to-roll (R2R) coating process.[2] The high ambipolar charge mobility in perovskite films enables optimal active layer thickness of a few hundreds of nanometers,[3−7] making printing of working PSCs more reproducible.[8] Meanwhile, a flat and flexible transparent electrode is highly desirable to be compatible with the R2R process. Most PSCs are built on transparent conductive oxides (TCOs) such as fluorine-doped tin oxide (FTO) or indium tin oxide (ITO),[9−19] which can cause the degradation of PSCs after bending because these TCOs are brittle materials.[20,21] Moreover, the transparent conductive electrode is the most expensive component in perovskite solar cells. Its cost is about 10 times of that of the perovskite layer in a PSC. Therefore, it is significant to explore alternative materials as the transparent electrode of PSCs. Recently, silver or gold thin films or silver nanowires have been used as a transparent electrode for perovskite solar cells.[18,22−24] However, iodide is quite corrosive for Ag or other metal nanostructures. To prepare metal nanowires and assemble them for transparent electrode is also costly.

In this study, we investigated the application of methanesulfonic acid (MSA)-treated poly(3,4-ethylenedioxythiophene):polystyrenesulfonate (PEDOT:PSS) as the transparent electrode of organo-lead halide perovskite solar cells. The chemical structures of MSA and PEDOT:PSS are shown in Chart 1. PEDOT:PSS is the most successful conducting polymer because of its solution processability, high transparency in the visible range, and excellent thermal stability. It has been reported that treatment of PEDOT:PSS films with an acid such as sulfuric acid and MSA can improve the conductivity to be comparable to that of ITO.[25−27] However,

Chart 1. Chemical Structure of PEDOT:PSS and Methanesulfonic Acid

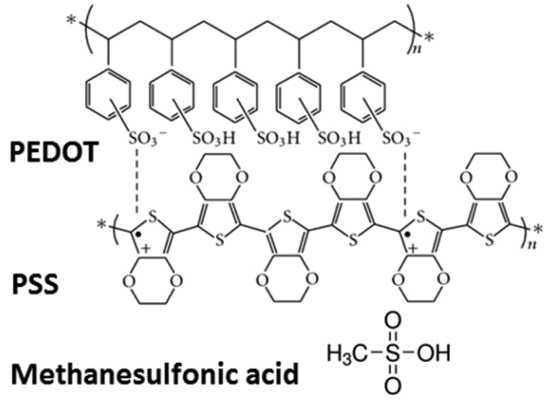

Received: April 13, 2015
Accepted: July 1, 2015
Published: July 1, 2015

DOI: 10.1021/acsami.5b03171
ACS Appl. Mater. Interfaces 2015, 7, 15314−15320

sulfuric acid is corrosive, and it cannot be used to treat PEDOT:PSS films on plastic substrate. In this work, MSA-treated PEDOT:PSS films were prepared on both glass and flexible poly(ethylene terephthalate) (PET) substrates, and they were exploited as the transparent electrode of perovskite solar cells. The optimal power conversion efficiency (PCE) is close to 11% for the rigid PSCs with a PEDOT:PSS film on glass, and it is more than 8% for the flexible PSCs with PEDOT:PSS on PET. The flexible PSCs exhibit excellent mechanical flexibility in the bending test.

2. EXPERIMENTAL DETAILS

2.1. Materials and Chemicals. Patterned ITO glass substrates (10 Ω sq^{-1}) were supplied by NSG group. PEDOT:PSS (Clevios P VP Al 4083 and Clevios PH 1000, Lot no. 2014P0146) aqueous solutions were purchased from Heraeus Holding GmbH. MAI was obtained from Dyesol, Ltd. [6,6]-phenyl-C61-butyric acid methyl ester (PCBM) was bought from Nano-C, Inc. Other materials, including lead(II) iodide (PbI_2 powder, 99% purity, and PbI_2 beads, 99.999% purity), lead(II) chloride ($PbCl_2$ powder, 99.999% purity), dimethyl sulfoxide (DMSO, anhydrous, ≥99.9% purity), γ-butyrolactone (GBL, ≥99% purity), bathocuproine (BCP), rhodamine 101 inner salt, LiF (≥99% purity), chlorobenzene (anhydrous, 99.8% purity), and isopropanol (IPA, anhydrous, 99.5% purity), were supplied by Sigma-Aldrich. All materials are used without further purification.

2.2. MSA Treatment of PEDOT:PSS Films. The glass substrates with a dimension of 1.5 × 1.5 cm^2 were cleaned sequentially with detergent, deionized (DI) water, acetone, and IPA. PEDOT:PSS films were prepared by spin coating the PEDOT:PSS (Clevios PH 1000) aqueous solution on the glass substrates. The PEDOT:PSS films were dried at 110 °C on a hot plate for 40 min. The acid treatment was carried out by dropping 100 μL of 8 M MSA aqueous solution on each PEDOT:PSS film at 160 °C on a hot plate. The films dried after about 3 min. They were then cooled to room temperature and rinsed with DI water by immersing the PEDOT:PSS films into DI water three times and IPA once, followed by drying at 160 °C.

2.3. Material Characterizations. The conductivities of the polymer films were measured by the Van der Pauw four-point probe technique with a Keithley 2400 source/meter. The electrical contacts were made by pressing indium on the four corners of each PEDOT:PSS film on glass substrate. Film thickness was determined by a surface profilometer (KLA Tencor, Alpha-Step IQ). UV−vis absorption spectra were recorded with a Shimadzu UV-1800 spectrophotometer. UPS and XPS were acquired with a Kratos Axis Ultra X-ray photoelectron spectroscope (Kratos Analytical) equipped with a monochromatized Al Kα X-ray source. AFM images were acquired using a Veeco NanoScope IV Multi-Mode AFM operated in tapping mode. SEM images were obtained with a Hitachi S-4100 scanning electron microscope. XRD patterns were acquired using a Bruker D8 Advance XRD Instrument.

2.4. Fabrication and Characterization of Perovskite Solar Cells. Patterned ITO glass substrates were cleaned sequentially in detergent, DI water, acetone, and IPA by sonication for 20 min. After drying under a N_2 stream, substrates were further treated with UV−ozone for 15 min. MSA-PEDOT:PSS on either glass or PET was patterned, and an indium bud was pressed onto the film to serve as the electrical contact. A PEDOT:PSS buffer layer with a thickness of ∼30 nm was prepared by spin coating Clevios P VP Al 4083 on the transparent electrode at 8000 rpm for 1 min and subsequently annealed at 140 °C for 10 min in air. The substrates with PEDOT:PSS were then transferred into a glovebox filled with highly pure N_2. The perovskite layer was formed by spin coating a solution consisting of 0.14 M $PbCl_2$, 1.26 M PbI_2, and 1.3 M MAI in cosolvent DMSO:GBL (3:7 v/v ratio) at 1000 rpm for 20 s, and then at 3500 rpm for 60 s. At 50 s after the start of the spin coating, 1 mL of toluene was dripped. Then, they were annealed at 100 °C for 20 min. The thickness of the perovskite thin films was around 300 nm. The PCBM layer with a thickness of about 55 nm was deposited by spin coating a chlorobenzene solution of 20 mg mL^{-1} PCBM at 2000 rpm for 40s. The interfacial layer was prepared on PCBM by spin coating an IPA solution of 0.05 wt % rhodamine 101. The other layers such as 30 nm of C60, 10 nm of BCP, 0.5 nm of rhodamine 101, and 0.8 nm of LiF were thermally evaporated in a vacuum of $<1 \times 10^{-6}$ mbar. The devices were completed by thermal deposition of a 100 nm thick layer of Ag. Each device had an area of 0.11 cm^2. The perovskite solar cells fabricated on glass were encapsulated with cover glass slides in the glovebox, whereas the flexible PSCs were not encapsulated. The photovoltaic performance of the PSCs was tested in air with a computer-programmed Keithley 2400 source/meter and a Newport's Oriel class A solar simulator, which simulated the AM 1.5G sunlight with energy density of 100 mW cm^{-2} and was certified to the JIS C 8912 standard. IPCEs of PSCs were measured with a 300 W xenon lamp (Oriel 6258) and a Cornerstone 260 Oriel 74125 monochromator. In the bending tests, the flexible PSCs were deformed manually to a bend radius of 2 mm at a frequency of 1 Hz.

3. RESULTS AND DISCUSSION

Highly conductive PEDOT:PSS films were used to replace TCO as the transparent electrode of PSCs. They were prepared by the following process. At first, PEDOT:PSS films were prepared by spin coating a commercial PEDOT:PSS solution on 1.5 × 1.5 cm^2 glass or PET substrates at various spin speeds. They were subsequently annealed at 120 °C on a hot plate for 40 min in air. The PEDOT:PSS films were treated with MSA to enhance the conductivity.[25] PEDOT:PSS treated with methanesulfonic acid is denoted as MSA-PEDOT:PSS in this paper. Polymer films with multiple MSA-PEDOT:PSS layers were also prepared by repeating the above processes for multiple cycles. MSA is used to treat PEDOT:PSS because MSA is a mild acid that can be readily rinsed away after the treatment. Although a strong acid like sulfuric acid can also improve significantly the conductivity of PEDOT:PSS,[27] it is not applicable for PEDOT:PSS on PET.

The MSA treatment significantly enhanced the conductivity of the PEDOT:PSS films. Table 1 lists the conductivity, sheet resistance, and transmittance at 550 nm of the pristine PEDOT:PSS film and MSA-PEDOT:PSS films with different thicknesses. The different thicknesses for MSA-PEDOT:PSS films were obtained by adjusting the spin coating rate. The electrical conductivity of the pristine films is around 0.3 S cm^{-1}. It can be enhanced drastically to be close to 2000 S cm^{-1} after the MSA treatment. The conductivity for the double-layer PEDOT:PSS films is higher than 2500 S cm^{-1}, much higher than that of the single-layer MSA-PEDOT:PSS films. It can be attributed to the double MSA treatments for the bottom PEDOT:PSS layer in the double-layer PEDOT:PSS films. The

Table 1. Conductivity (σ), Sheet Resistance (R), and Transmittance (T) at 550 nm of Pristine PEDOT:PSS Thin Film and MSA-PEDOT:PSS Films of Different Thicknesses (d)

condition	σ (S cm^{-1})	d (nm)	R (Ω sq^{-1})[a]	T (%)[b]
pristine PEDOT:PSS, 1 layer	0.3	75	446211	97
MSA-PEDOT:PSS, 1 layer	1762	67	85	93
MSA-PEDOT:PSS, 1 layer	1679	50	119	95
MSA-PEDOT:PSS, 1 layer	1850	39	139	96
MSA-PEDOT:PSS, 1 layer	1814	31	178	97
MSA-PEDOT:PSS, 2 layer	2540	79	50	92

[a]Sheet resistance (R) was derived by using Van der Pauw method. [b]Glass was used as the reference.

DOI: 10.1021/acsami.5b03171
ACS Appl. Mater. Interfaces 2015, 7, 15314−15320

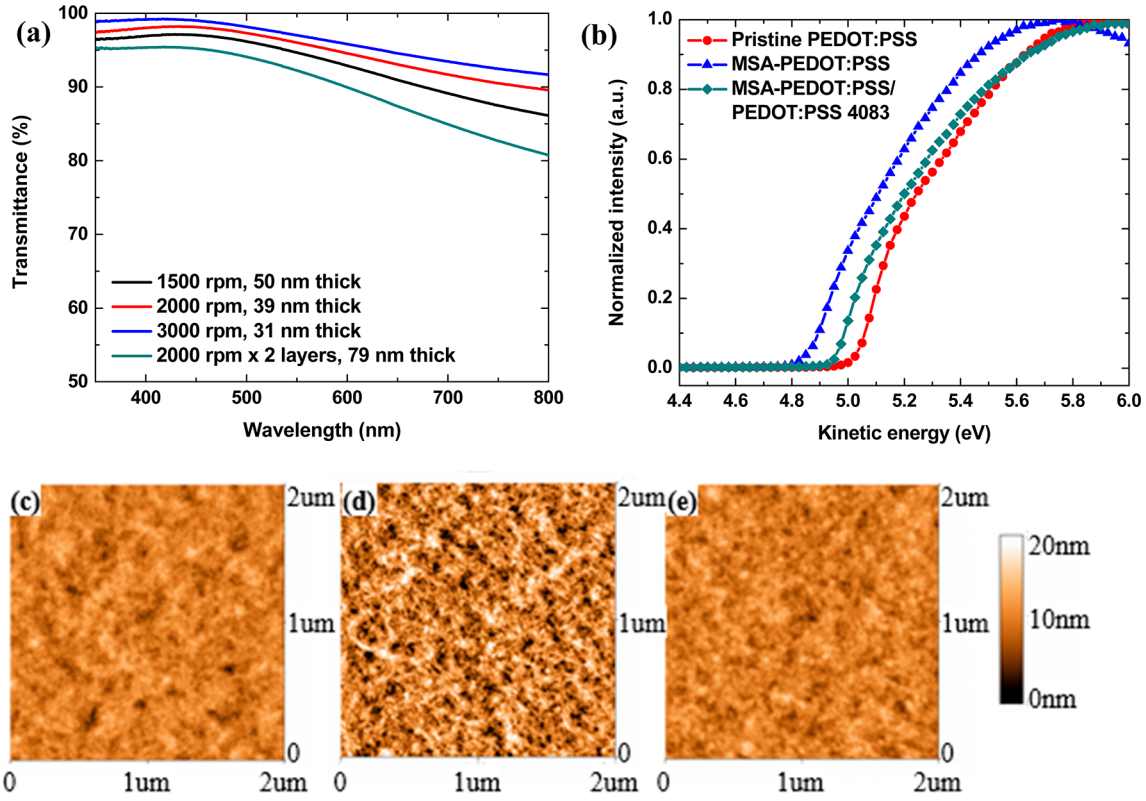

Figure 1. (a) UV−vis transmittance spectra of MSA-PEDOT:PSS films of different thicknesses on glass. (b) Ultraviolet photoelectron spectroscopy of pristine PEDOT:PSS, MSA-PEDOT:PSS, and MSA-PEDOT:PS covered with PEDOT:PSS 4083. AFM height images of (c) a pristine PEDOT:PSS film, (d) a MSA-PEDOT:PSS film, and (e) a MSA-PEDOT:PSS film covered with PEDOT:PSS 4083. The image size is 2 × 2 μm.

conductivity enhancement can be ascribed to the MSA-induced phase segregation between PSS and PEDOT in the PEDOT:PSS film and coil-to-linear conformational change of the PEDOT chains.[25−30]

The MSA treatment hardly affects the transmittance of the PEDOT:PSS films in the visible range. The transmittance spectra of MSA-PEDOT:PSS films with various thicknesses are presented in Figure 1a. For the single-layer MSA-PEDOT:PSS films, the optical transmittance at 550 nm is between 93 and 97%. The transmittance of the double-layer MSA-PEDOT:PSS film with a thickness of 79 nm is slightly lower, but it is still higher than 90% at 550 nm. The double-layer MSA-PEDOT:PSS thin film exhibits a sheet resistance of 50 Ω sq^{-1} and a transmittance of 92% at 550 nm, which are comparable to the performance of ITO on PET.[31] Therefore, MSA-PEDOT:PSS films can be used to replace ITO as the transparent electrode, particularly as the flexible transparent electrode.

Apart from the sheet resistance and transmittance, the surface properties, including the work function and the surface morphology, of the MSA-PEDOT:PSS films are also crucial for the their application as the transparent electrode of PSCs. Ultraviolet photoelectron spectroscopy (UPS) suggests the pristine PEDOT:PSS shows a work function of 5.0 eV (Figure 1b). The MSA treatment slightly lowers the work function by about 0.2 to 4.8 eV. Coating a PEDOT:PSS 4083 layer on MSA-PEDOT:PSS (MSA-PEDOT:PSS/PEDOT:PSS 4083) recovers the work function to 4.9 eV. A slight reduction in work function of PEDOT:PSS film was observed after sorbitol treatment.[32] This is related to the partial removal of PSS component in the PEDOT:PSS film.[33] The MSA treatment makes the PEDOT:PSS films rougher (Figure 1c,d). As revealed by the AFM images, the pristine PEDOT:PSS film has a smooth surface with a root-mean-square roughness (R_{rms}) of 1.6 nm. After the MSA treatment, small domains and entangled nanowires can be observed. The R_{rms} value increases to 2.9 nm, almost twice of that of the pristine PEDOT:PSS film. Coating a layer of PEDOT:PSS 4083 on the MSA-PEDOT:PSS film smooths the surface (Figure 1e). The R_{rms} value is 1.7 nm for MSA-PEDOT:PSS/PEDOT:PSS 4083.

A layer of $CH_3NH_3PbCl_xI_{3-x}$ was coated on an MSA-PEDOT:PSS or an MSA-PEDOT:PSS/PEDOT:PSS 4083 film. Figure 2a,b shows the SEM images of $CH_3NH_3PbCl_xI_{3-x}$ layers on the two films. Previously, we found that introducing slightly more PbI_2 relative to methylammonium iodide (MAI) could limit the perovskite crystal growth as well as passivate the grain boundaries of perovskite crystals, thus reducing the charge recombination.[34] In the SEM images, the darker phase is attributed to perovskite crystals, whereas the lighter phase is due to excess PbI_2, which is less conducting. Comparing Figure 2a,b, there is more PbI_2 phase in the former than latter. The perovskite crystals in Figure 2a are not as large and well-shaped as those in Figure 2b. This indicates that the conversion from PbI_2 to perovskite is less complete on MSA-PEDOT:PSS substrate than on MSA-PEDOT:PSS/PEDOT:PSS 4083 film. XRD patterns provide further evidence (Figure 2c). The peak at 12.8° originates from PbI_2 crystal, whereas the peak at 14.4° belongs to perovskite. The ratios between these two peaks are 0.38 and 0.26 for the perovskite layer on MSA-PEDOT:PSS substrate without and with the PEDOT:PSS 4083 layer, respectively. Thus, there is more unreacted PbI_2 in the perovskite layer when it is deposited on a MSA-PEDOT:PSS

DOI: 10.1021/acsami.5b03171
ACS Appl. Mater. Interfaces 2015, 7, 15314−15320

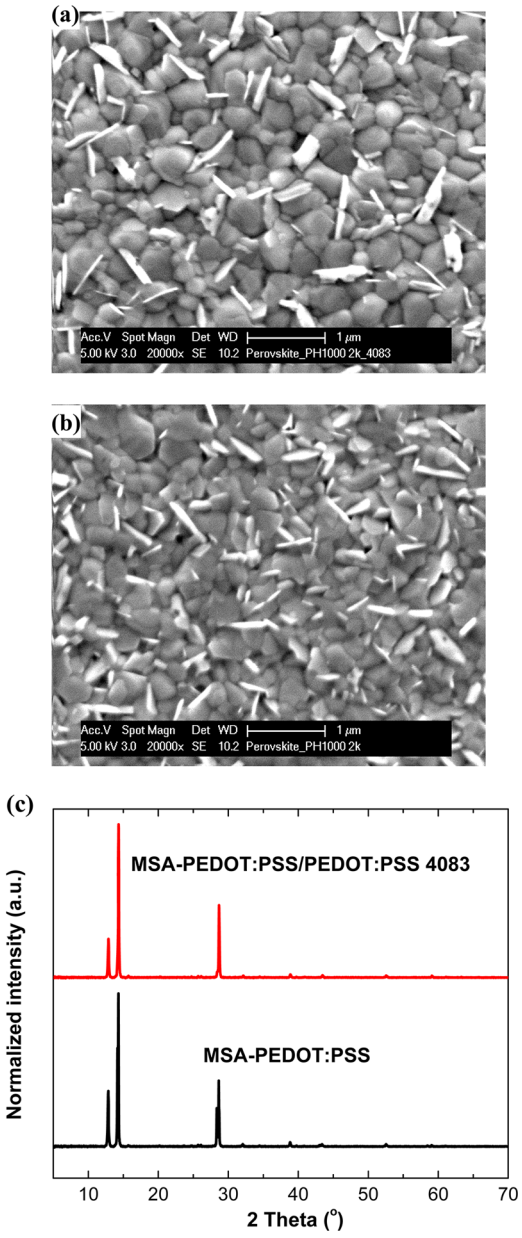

Figure 2. SEM images of $CH_3NH_3PbCl_xI_{3-x}$ perovskite layer on a (a) MSA-PEDOT:PSS film and (b) PEDOT:PSS 4083 coated MSA-PEDOT:PSS film. (c) XRD pattern of the perovskite film on MSA-PEDOT:PSS film without or with PEDOT:PSS 4083 coating. Scale bar in the SEM images is 1 μm.

film. This is probably related to the surface properties of the polymer films. MSA-PEDOT:PSS is more hydrophobic than pristine PEDOT:PSS because of the removal of hydrophilic PSSH chains, but PEDOT:PSS 4083 is more hydrophilic because the PSS/PEDOT weight ratios are 2.5 and 6 for PEDOT:PSS PH1000 and PEDOT:PSS 4083, respectively. PbI_2, $PbCl_2$, CH_3NH_3I, and $CH_3NH_3PbCl_xI_{3-x}$ are ionic compounds, and the solvents to coat the $CH_3NH_3PbCl_xI_{3-x}$ layer are also polar solvents. A polar solution can wet readily a hydrophilic surface and bring the solutes to the substrate, where nucleation can take place and crystal growth can happen subsequently. Therefore, a hydrophilic layer beneath may favor the conversion of the precursors to $CH_3NH_3PbCl_xI_{3-x}$.

Planar PSCs were fabricated using MSA-PEDOT:PSS on glass as the transparent electrode. The schematic device architecture is shown in Figure 3a. The current (J)−voltage (V) curve for an optimal device is shown in Figure 3b. The $J-V$ curve of a control device with ITO as the transparent electrode is also presented for comparison. The photovoltaic performances are summarized in Table 2. The best PSC fabricated on MSA-PEDOT:PSS/glass shows a short-circuit current density (J_{sc}) of 17.43 mA cm^{-2}, an open-circuit voltage (V_{oc}) of 0.97 V, an FF of 0.65, and a PCE of 11.0%. The photovoltaic performances are reproducible for the PSCs. The photovoltaic performances are not as high as that of the control device, which has a J_{sc} of 19.30 mA cm^{-2}, a V_{oc} of 1.10 V, an FF of 0.74, and a PCE of 15.6%. The photon-to-electron conversion efficiency (IPCE) spectra for the two devices are shown in Figure 3c. They suggest that the J_{sc} of the PSC with MSA-PEDOT:PSS being lower than that of the control PSC with ITO is mainly due to the light-to-electricity conversion in the near UV range. Presumably, the fact that the PSC with MSA-PEDOT:PSS has a photovoltaic efficiency lower than that of the control PSC with ITO is related to the conductivity of the transparent electrodes. Although an MSA-PEDOT:PSS film can have a conductivity of more than 2000 S cm^{-1}, it is still much lower than that of ITO on glass (~6000 S cm^{-1}). The sheet resistance of ITO on glass is about 10 Ω sq^{-1}.

PSCs were fabricated on MSA-PEDOT:PSS/glass without the PEDOT:PSS 4083 layer (Figure S1 and Table S1). In comparison with the characteristics of the device with the PEDOT:PSS 4083 layer, the V_{oc} and FF greatly decrease. This can be attributed to the lower work function of MSA-PEDOT:PSS than PEDOT:PSS 4083. Two other types of device architectures with different structures and materials for the electron collection were also investigated (Figures S2 and S3 and Table S2). Bathocuproine (BCP)/Ag and rhodamine 101/LiF/Ag were used for the electron collection of the two types of PSCs. These PSCs exhibited photovoltaic efficiencies of slightly lower than 10%.

Rhodamine 101 is used as an interlayer material for electron collection. It has an intrinsic dipole moment because of the positive and negative charges in the same molecule, and it has been used as the interlayer for electron collection in polymer solar cells.[35,36] Because the MSA-PEDOT:PSS layer is rough, a C_{60} layer is needed to lower the leakage current, but there is an energy barrier between the LUMO (−4.1 eV) of C_{60} and the Fermi level (−4.3 eV) of Ag, which suppresses the electron collection. Although LiF can reduce the energy barrier, a double-interlayer structure of rhodamine 101/LiF can make electron collection more efficient for PSCs with ITO as presented in our previous report.[34] However, when the rhodamine 101 layer is too thick, it will suppress electron collection. When it is too thin, its effect on reducing the energy barrier is not very effective because it cannot fully cover the surface of the C_{60} layer. We found that two thin rhodamine 101 layers, one above C_{60} and another below C_{60}, can effectively help electron collection for the PSCs with MSA-PEDOT:PSS.

Because PEDOT:PSS films have high mechanical flexibility, bending will not cause degradation in either optical or electrical properties. An MSA-PEDOT:PSS film is thus a good candidate as the transparent electrode of flexible optoelectronics. MSA-PEDOT:PSS films on PET substrate were exploited as the transparent electrode of flexible PSCs. Figure 4a shows a completed flexible perovskite solar cell that can be bent. The flexible PSC shows a remarkable PCE of 8.6%, with a J_{sc} of 17.15 mA cm^{-2}, a V_{oc} of 0.87 V, and an FF of 0.57. The flexible PSCs also have good reproducility in their photovoltaic

DOI: 10.1021/acsami.5b03171
ACS Appl. Mater. Interfaces 2015, 7, 15314−15320

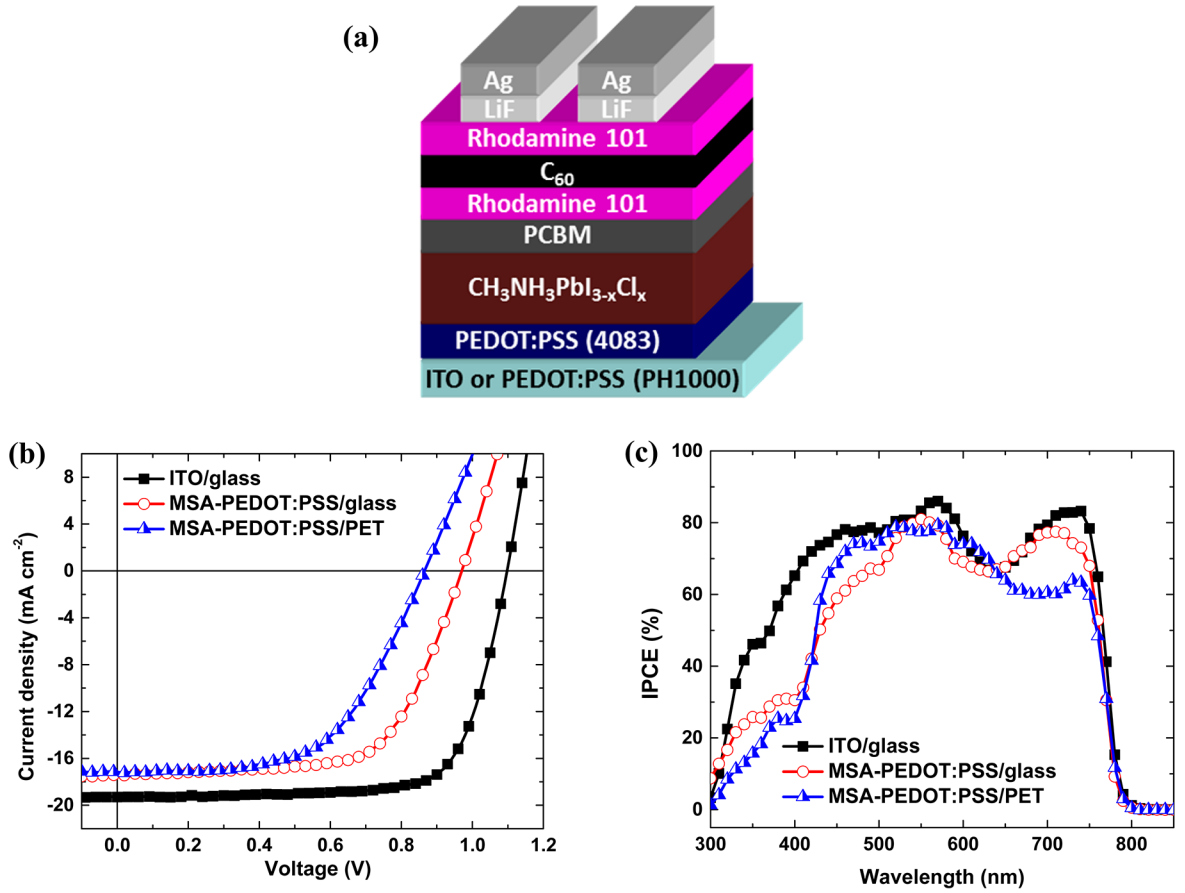

Figure 3. (a) Schematic architecture of PSCs. (b) $J-V$ characteristics and (c) IPCE spectra of PSCs with different transparent electrodes.

Table 2. Summary of Photovoltaic Parameters of PSCs with Different Transparent Electrodes

transparent electrode	J_{sc} (mA cm^{-2})	V_{oc} (V)	FF	PCE (%)
ITO/glass	19.30	1.10	0.74	15.6
	17.89 ± 0.58[a]	1.11 ± 0.02[a]	0.74 ± 0.02[a]	14.7 ± 0.4[a]
MSA-PEDOT:PSS/glass	17.43	0.97	0.65	11.0
	17.17 ± 0.64[a]	0.95 ± 0.02[a]	0.64 ± 0.02[a]	10.6 ± 0.3[a]
MSA-PEDOT:PSS/PET	17.15	0.87	0.57	8.6
	17.16 ± 0.65[a]	0.88 ± 0.02[a]	0.54 ± 0.03[a]	8.1 ± 0.3[a]

[a]Average values and standard deviations are calculated from 15 devices.

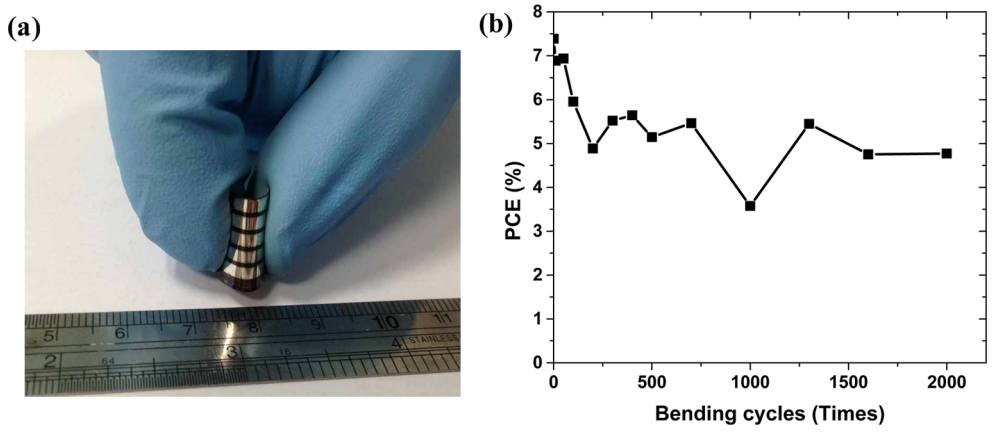

Figure 4. (a) Photo of a flexible PSC with MSA-PEDOT:PSS/PET. The PSC is deformed manually to a bend radius of 2 mm. (b) Variation of the PCE of a flexible PSC with the bending cycle.

DOI: 10.1021/acsami.5b03171
ACS Appl. Mater. Interfaces 2015, 7, 15314−15320

performance. To test the mechanical flexibility of the flexible PSCs, bending tests in air without encapsulation were carried out. The flexible PSCs were deformed manually to a bend radius of 2−3 mm, as shown in the inset of Figure 4b. Repeated bending at a frequency of 1 Hz causes the degradation of PCE from 7.5 to ∼5.5% during the first 500 cycles. The performance is then stabilized from the 500th to the 2000th cycle. Our result demonstrates that MSA-PEDOT:PSS/PET is a robust flexible transparent electrode alternative to TCO/PET, which most of flexible perovskite solar cells employed.[16,21,37−43] Bending can cause crack formation for the rigid TCO films.[20] Flexible PSCs with ITO/PET substrates were also reported in literature.[41,42] The authors found that the photovoltaic performane of those devices did not remarkably change after tens of bending tests and claimed that the ITO/PET substrate could be used for roll-to-roll fabrication of PSCs. There are some differences between those works and this work. First, the bend radius of this work is only 2 mm, much less than the bend radii in those works. A lower bend radius requires higher flexibility. Second, only tens of bending tests were performed to test the flexibility of the devices in those works. The cracks on TCO/PET gradually develop so that no remarkable effect can be observed for tens of bending tests. In this work, the bending tests were cycled for 2000 times.

4. CONCLUSIONS

MSA-PEDOT:PSS films can have a conductivity of more than 2000 S cm^{-1} and high transmittance in the visible range. MSA-PEDOT:PSS films are investigated as the transparent electrode of rigid and flexible PSCs. The optimized PSCs are 11.0 and 8.6% for the rigid PSCs with glass substrate and flexible PSCs with PET substrate, respectively. The flexible PSC can survive a small bending radius of 2 mm and retain more than 50% of initial PCE after repeated bending in air for 2000 bending cycles.

■ ASSOCIATED CONTENT

Supporting Information

Scheme of two different cell architectures, $J-V$ characteristics, and photovoltaic performance parameters of the perovskite solar cells employing these two cell architectures. The Supporting Information is available free of charge on the ACS Publications website at DOI: 10.1021/acsami.5b03171.

■ AUTHOR INFORMATION

Corresponding Author

*E-mail: mseoj@nus.edu.sg.

Notes

The authors declare no competing financial interest.

■ ACKNOWLEDGMENTS

We thank the financial support from the Ministry of Education, Singapore (R-284-000-113-112). K.S. is grateful to the Chongqing University for a grant (0212001104431).

■ REFERENCES

(1) Wang, K.; Liu, C.; Du, P.; Zhang, H.-L.; Gong, X. Efficient Perovskite Hybrid Solar Cells Through a Homogeneous High-Quality Organolead Iodide Layer. *Small* **2015**, n/a.

(2) Hwang, K.; Jung, Y.-S.; Heo, Y.-J.; Scholes, F. H.; Watkins, S. E.; Subbiah, J.; Jones, D. J.; Kim, D.-Y.; Vak, D. Toward Large Scale Roll-to-Roll Production of Fully Printed Perovskite Solar Cells. *Adv. Mater.* **2015**, *27*, 1241−1247.

(3) Stranks, S. D.; Eperon, G. E.; Grancini, G.; Menelaou, C.; Alcocer, M. J. P.; Leijtens, T.; Herz, L. M.; Petrozza, A.; Snaith, H. J. Electron-Hole Diffusion Lengths Exceeding 1 Micrometer in an Organometal Trihalide Perovskite Absorber. *Science* **2013**, *342*, 341−344.

(4) Xing, G.; Mathews, N.; Sun, S.; Lim, S. S.; Lam, Y. M.; Grätzel, M.; Mhaisalkar, S.; Sum, T. C. Long-Range Balanced Electron- and Hole-Transport Lengths in Organic-Inorganic $CH_3NH_3PbI_3$. *Science* **2013**, *342*, 344−347.

(5) Dong, Q.; Fang, Y.; Shao, Y.; Mulligan, P.; Qiu, J.; Cao, L.; Huang, J. Electron-Hole Diffusion Lengths >175 μm in Solution Grown $CH_3NH_3PbI_3$ Single Crystals. *Science* **2015**, *347*, 967−970.

(6) Wang, K.; Liu, C.; Du, P.; Zheng, J.; Gong, X. Bulk Heterojunction Perovskite Hybrid Solar Cells with Large Fill Factor. *Energy Environ. Sci.* **2015**, *8*, 1245−1255.

(7) Wang, K.; Liu, C.; Du, P.; Chen, L.; Zhu, J.; Karim, A.; Gong, X. Efficiencies of Perovskite Hybrid Solar Cells Influenced by Film Thickness and Morphology of $CH_3NH_3PbI_{3-x}Cl_x$ Layer. *Org. Electron.* **2015**, *21*, 19−26.

(8) Sun, K.; Xiao, Z.; Lu, S.; Zajaczkowski, W.; Pisula, W.; Hanssen, E.; White, J. M.; Williamson, R. M.; Subbiah, J.; Ouyang, J.; Holmes, A. B.; Wong, W. W. H.; Jones, D. J. A Molecular Nematic Liquid Crystalline Material for High-Performance Organic Photovoltaics. *Nat. Commun.* **2015**, *6*, 6013.

(9) Liu, C.; Wang, K.; Du, P.; Meng, T.; Yu, X.; Cheng, S. Z. D.; Gong, X. High Performance Planar Heterojunction Perovskite Solar Cells with Fullerene Derivatives as the Electron Transport Layer. *ACS Appl. Mater. Interfaces* **2015**, *7*, 1153−1159.

(10) Burschka, J.; Pellet, N.; Moon, S.-J.; Humphry-Baker, R.; Gao, P.; Nazeeruddin, M. K.; Gratzel, M. Sequential Deposition as a Route to High-Performance Perovskite-Sensitized Solar Cells. *Nature* **2013**, *499*, 316−319.

(11) Jeng, J.-Y.; Chiang, Y.-F.; Lee, M.-H.; Peng, S.-R.; Guo, T.-F.; Chen, P.; Wen, T.-C. $CH_3NH_3PbI_3$ Perovskite/Fullerene Planar-Heterojunction Hybrid Solar Cells. *Adv. Mater.* **2013**, *25*, 3727−3732.

(12) Conings, B.; Baeten, L.; De Dobbelaere, C.; D'Haen, J.; Manca, J.; Boyen, H.-G. Perovskite-Based Hybrid Solar Cells Exceeding 10% Efficiency with High Reproducibility Using a Thin Film Sandwich Approach. *Adv. Mater.* **2014**, *26*, 2041−2046.

(13) Xiao, Z.; Dong, Q.; Bi, C.; Shao, Y.; Yuan, Y.; Huang, J. Solvent Annealing of Perovskite-Induced Crystal Growth for Photovoltaic-Device Efficiency Enhancement. *Adv. Mater.* **2014**, *26*, 6503−6509.

(14) Chen, Y.; Chen, T.; Dai, L. Layer-by-Layer Growth of $CH_3NH_3PbI_{3-x}Cl_x$ for Highly Efficient Planar Heterojunction Perovskite Solar Cells. *Adv. Mater.* **2015**, *27*, 1053−1059.

(15) Jeon, N. J.; Noh, J. H.; Kim, Y. C.; Yang, W. S.; Ryu, S.; Seok, S. I. Solvent Engineering for High-Performance Inorganic−Organic Hybrid Perovskite Solar Cells. *Nat. Mater.* **2014**, *13*, 897−903.

(16) Dkhissi, Y.; Huang, F.; Rubanov, S.; Xiao, M.; Bach, U.; Spiccia, L.; Caruso, R. A.; Cheng, Y.-B. Low Temperature Processing of Flexible Planar Perovskite Solar Cells with Efficiency Over 10%. *J. Power Sources* **2015**, *278*, 325−331.

(17) Chen, Y.; Zhao, Y.; Liang, Z. Non-Thermal Annealing Fabrication of Efficient Planar Perovskite Solar Cells with Inclusion of NH_4Cl. *Chem. Mater.* **2015**, *27*, 1448−1451.

(18) Min, J.; Zhang, Z.-G.; Hou, Y.; Ramirez Quiroz, C. O.; Przybilla, T.; Bronnbauer, C.; Guo, F.; Forberich, K.; Azimi, H.; Ameri, T.; Spiecker, E.; Li, Y.; Brabec, C. J. Interface Engineering of Perovskite Hybrid Solar Cells with Solution-Processed Perylene−Diimide Heterojunctions toward High Performance. *Chem. Mater.* **2015**, *27*, 227−234.

(19) Zhang, H.; Azimi, H.; Hou, Y.; Ameri, T.; Przybilla, T.; Spiecker, E.; Kraft, M.; Scherf, U.; Brabec, C. J. Improved High-Efficiency Perovskite Planar Heterojunction Solar Cells via Incorporation of a Polyelectrolyte Interlayer. *Chem. Mater.* **2014**, *26*, 5190−5193.

(20) Poorkazem, K.; Liu, D.; Kelly, T. L. Fatigue Resistance of a Flexible, Efficient, and Metal Oxide-Free Perovskite Solar Cell. *J. Mater. Chem. A* **2015**, *3*, 9241−9248.

DOI: 10.1021/acsami.5b03171
ACS Appl. Mater. Interfaces 2015, 7, 15314−15320

(21) Kim, B. J.; Kim, D. H.; Lee, Y.-Y.; Shin, H.-W.; Han, G. S.; Hong, J. S.; Mahmood, K.; Ahn, T. K.; Joo, Y.-C.; Hong, K. S.; Park, N.-G.; Lee, S.; Jung, H. S. Highly Efficient and Bending Durable Perovskite Solar Cells: Toward a Wearable Power Source. *Energy Environ. Sci.* **2015**, *8*, 916−921.
(22) Lee, M.; Jo, Y.; Kim, D. S.; Jun, Y. Flexible Organo-Metal Halide Perovskite Solar Cells on a Ti Metal Substrate. *J. Mater. Chem. A* **2015**, *3*, 4129−4133.
(23) Bailie, C. D.; Christoforo, M. G.; Mailoa, J. P.; Bowring, A. R.; Unger, E. L.; Nguyen, W. H.; Burschka, J.; Pellet, N.; Lee, J. Z.; Gratzel, M.; Noufi, R.; Buonassisi, T.; Salleo, A.; McGehee, M. D. Semi-Transparent Perovskite Solar Cells for Tandems with Silicon and CIGS. *Energy Environ. Sci.* **2015**, *8*, 956−963.
(24) Della Gaspera, E.; Peng, Y.; Hou, Q.; Spiccia, L.; Bach, U.; Jasieniak, J. J.; Cheng, Y.-B. Ultra-Thin High Efficiency Semi-transparent Perovskite Solar Cells. *Nano Energy* **2015**, *13*, 249−257.
(25) Ouyang, J. Solution-Processed PEDOT:PSS Films with Conductivities as Indium Tin Oxide through a Treatment with Mild and Weak Organic Acids. *ACS Appl. Mater. Interfaces* **2013**, *5*, 13082−13088.
(26) Xia, Y. J.; Sun, K.; Ouyang, J. Y. Highly Conductive Poly(3,4-ethylenedioxythiophene): poly(styrene sulfonate) Films Treated with an Amphiphilic Fluoro Compound as the Transparent Electrode of Polymer Solar Cells. *Energy Environ. Sci.* **2012**, *5*, 5325−5332.
(27) Xia, Y. J.; Sun, K.; Ouyang, J. Y. Solution-Processed Metallic Conducting Polymer Films as Transparent Electrode of Optoelectronic Devices. *Adv. Mater.* **2012**, *24*, 2436−2440.
(28) Ouyang, J.; Chu, C. W.; Chen, F. C.; Xu, Q.; Yang, Y. High-Conductivity Poly(3,4-ethylenedioxythiophene):Poly(styrene sulfonate) Film and Its Application in Polymer Optoelectronic Devices. *Adv. Funct. Mater.* **2005**, *15*, 203−208.
(29) Sun, K.; Xia, Y. J.; Ouyang, J. Y. Improvement in the Photovoltaic Efficiency of Polymer Solar Cells by Treating the Poly(3,4-ethylenedioxythiophene): poly(styrenesulfonate) Buffer Layer with Co-solvents of Hydrophilic Organic Solvents and Hydrophobic 1,2-dichlorobenzene. *Sol. Energy Mater. Sol. Cells* **2012**, *97*, 89−96.
(30) Sun, K.; Zhang, S.; Li, P.; Xia, Y.; Zhang, X.; Du, D.; Isikgor, F.; Ouyang, J. Review on Application of PEDOTs and PEDOT:PSS in Energy Conversion and Storage Devices. *J. Mater. Sci.: Mater. Electron.* **2015**, *26*, 4438−4462.
(31) Na, S. I.; Kim, S. S.; Jo, J.; Kim, D. Y. Efficient and Flexible ITO-Free Organic Solar Cells Using Highly Conductive Polymer Anodes. *Adv. Mater.* **2008**, *20*, 4061−4067.
(32) Nardes, A. M.; Kemerink, M.; de Kok, M. M.; Vinken, E.; Maturova, K.; Janssen, R. A. J. Conductivity, Work Function, and Environmental Stability of PEDOT:PSS Thin Films Treated with Sorbitol. *Org. Electron.* **2008**, *9*, 727−734.
(33) Sapp, S.; Luebben, S.; Losovyj, Y. B.; Jeppson, P.; Schulz, D. L.; Caruso, A. N. Work Function and Implications of Doped Poly(3,4-ethylenedioxythiophene)-co-poly(ethylene glycol). *Appl. Phys. Lett.* **2006**, *88*, 152107.
(34) Sun, K.; Chang, J.; Isikgor, F.; Li, P.; Ouyang, J. Efficiency Enhancement of Planar Perovskite Solar Cells by Adding Zwitterion/LiF Double Interlayers for Electron Collection. *Nanoscale* **2015**, *7*, 896−900.
(35) Sun, K.; Zhao, B. M.; Kumar, A.; Zeng, K. Y.; Ouyang, J. Y. Highly Efficient, Inverted Polymer Solar Cells with Indium Tin Oxide Modified with Solution-Processed Zwitterions as the Transparent Cathode. *ACS Appl. Mater. Interfaces* **2012**, *4*, 2009−2017.
(36) Sun, K.; Zhao, B.; Murugesan, V.; Kumar, A.; Zeng, K.; Subbiah, J.; Wong, W. W. H.; Jones, D. J.; Ouyang, J. High-performance Polymer Solar Cells with a Conjugated Zwitterion by Solution Processing or Thermal Deposition as the Electron-collection Interlayer. *J. Mater. Chem.* **2012**, *22*, 24155−24165.
(37) Docampo, P.; Ball, J. M.; Darwich, M.; Eperon, G. E.; Snaith, H. J. Efficient Organometal Trihalide Perovskite Planar-Heterojunction Solar Cells on Flexible Polymer Substrates. *Nat. Commun.* **2013**, *4*, 2761.
(38) Chiang, Y.-F.; Jeng, J.-Y.; Lee, M.-H.; Peng, S.-R.; Chen, P.; Guo, T.-F.; Wen, T.-C.; Hsu, Y.-J.; Hsu, C.-M. High Voltage and Efficient Bilayer Heterojunction Solar Cells Based on an Organic-Inorganic Hybrid Perovskite Absorber with a Low-Cost Flexible Substrate. *Phys. Chem. Chem. Phys.* **2014**, *16*, 6033−6040.
(39) Jung, J. W.; Williams, S. T.; Jen, A. K. Y. Low-Temperature Processed High-Performance Flexible Perovskite Solar Cells via Rationally Optimized Solvent Washing Treatments. *RSC Adv.* **2014**, *4*, 62971−62977.
(40) Liu, D.; Kelly, T. L. Perovskite Solar Cells with a Planar Heterojunction Structure Prepared Using Room-Temperature Solution Processing Techniques. *Nat. Photonics* **2013**, *8*, 133−138.
(41) Roldan-Carmona, C.; Malinkiewicz, O.; Soriano, A.; Minguez Espallargas, G.; Garcia, A.; Reinecke, P.; Kroyer, T.; Dar, M. I.; Nazeeruddin, M. K.; Bolink, H. J. Flexible High Efficiency Perovskite Solar Cells. *Energy Environ. Sci.* **2014**, *7*, 994−997.
(42) You, J.; Hong, Z.; Yang, Y.; Chen, Q.; Cai, M.; Song, T.-B.; Chen, C.-C.; Lu, S.; Liu, Y.; Zhou, H.; et al. Low-Temperature Solution-Processed Perovskite Solar Cells with High Efficiency and Flexibility. *ACS Nano* **2014**, *8*, 1674−1680.
(43) Ryu, S.; Seo, J.; Shin, S. S.; Kim, Y. C.; Jeon, N. J.; Noh, J. H.; Seok, S. I. Fabrication of Metal-Oxide-Free $CH_3NH_3PbI_3$ Perovskite Solar Cells Processed at Low Temperature. *J. Mater. Chem. A* **2015**, *3*, 3271−3275.

DOI: 10.1021/acsami.5b03171
ACS Appl. Mater. Interfaces 2015, 7, 15314−15320